



Impact of Primarily Emitted Oxygenated Volatile Organic Compounds on Ozone Formation in the Yangtze River Delta Region

Xun Li¹, Xuan Li¹, Rusha Yan², Yaqin Gao², Kangjia Gong¹, Hongli Wang², Momei Qin¹, Jianlin Hu¹, Jingyi Li^{1,*}

¹Jiangsu Key Laboratory of Atmospheric Environment Monitoring and Pollution Control, Collaborative Innovation Center of Atmospheric Environment and Equipment Technology, School of Environmental Science and Engineering, Nanjing University of Information Science & Technology, Nanjing 210044, China

10 ²State Environmental Protection Key Laboratory of Formation and Prevention of Urban Air Pollution Complex, Shanghai Academy of Environmental Sciences, Shanghai 200233, China

*Correspondence to: Jingyi Li (jingyili@nuist.edu.cn)

Abstract. Oxygenated volatile organic compounds (OVOCs) play a crucial role in tropospheric radical chemistry, which in turn enhances atmospheric oxidation capacity and drives the formation of secondary pollutants. However, large uncertainties in their emissions pose challenges to accurately assessing their impacts on regional air quality. This study incorporates updated anthropogenic emission inventories, featuring source-resolved OVOC profiles derived from measurements and literature, into the Community Multiscale Air Quality (CMAQ) model to improve OVOC simulations over the Yangtze River Delta (YRD) region. The model well captured the diurnal and seasonal variations of most OVOCs, especially carbonyls. Primary emissions accounted for 30-70% of total OVOC concentrations, with higher contributions during colder months due to weaker atmospheric oxidation capacity. Hydroperoxyl radicals (HO₂), the primary oxidant driving NO-to-NO₂ conversion in urban areas, were substantially produced through OVOC photooxidation. Of the HO2 produced by this process, approximately 15-40% originated from directly emitted OVOCs rather than from secondary OVOCs formed via VOC oxidation. Sensitivity analysis further indicated that key emitted OVOCs contributed to ozone formation at levels comparable to traditional VOC precursors. These findings underscore the critical yet often overlooked role of primary OVOC emissions in urban ozone formation, highlighting the need for more comprehensive assessments in regions like the YRD.





1 Introduction

30 Tropospheric ozone (O3) pollution arises from the continuous oxidation of nitric oxide (NO) to nitrogen dioxide (NO2) by hydroperoxyl (HO2) and organic peroxy (RO2) radicals. These radicals are generated through initiation processes, such as the photolysis of oxygenated volatile organic compounds (OVOCs) and the ozonolysis of unsaturated VOCs, and are subsequently recycled via radical chain propagation reactions. Under polluted conditions, OVOC photolysis can become a dominant radical source, substantially enhancing O₃ formation (Yang et al., 2024; Tan et al., 2019b; Xue et al., 2016; Qu et al., 35 2021; Stockwell et al., 2021). Box model simulations constrained by observed OVOC concentrations have significantly improved the simulated HO2, RO2, and hydroxyl (OH) radical levels (Wang et al., 2022b; Wang et al., 2023; Yang et al., 2022), underscoring the critical role of OVOCs in radical budgets. These findings highlight the need for accurate representation of OVOC speciation and concentrations in 40 air quality models to support effective O3 mitigation strategies. Significant discrepancies persist between modeled and observed OVOC concentrations. Box models driven by observed pollutant concentrations, which reflect the chemically aged residuals of reactive species, may misrepresent OVOC variations and thus deviate from observations. As OVOCs are generated through the multi-step oxidation of VOCs, chemical transport model biases are strongly influenced by uncertainties in VOC precursor emissions, which largely depend on the accuracy of activity data and emission factors (Smith et al., 2022). In addition, the chemical production and loss pathways of OVOCs play a critical role. For example, the yield of formaldehyde (HCHO), the simplest aldehyde, is highly sensitive to isoprene chemistry and can directly affect ozone production rates (Marvin et al., 2017). The uptake of small aldehydes and organic acids by deliquesced particles represents an important source of secondary organic aerosols (SOAs). While the SOA formation mechanisms of glyoxal and methylglyoxal have been extensively studied, the contribution of other small aldehydes and organic acids remains poorly quantified due to limited studies and sparse observational data (Gkatzelis et al., 2021). Another important yet often overlooked factor lies in the uncertainties associated with OVOC emissions. Only a limited number of OVOC species are explicitly represented in most emission inventories, partially due to the constraints of traditional detection techniques (Pfannerstill et al., 2023; Wang et al., 2022a). Moreover, VOC and OVOC sources are typically aggregated into broad categories (e.g., industry,

transportation, residential, and power), and their total emissions are generally reported on a monthly or

60

65

70

75





annual basis. This introduces substantial uncertainties in temporal and spatial allocations, particularly for industrial sources that encompass diverse processes and exhibit sector-specific characteristics (Hu et al., 2025). In addition, emerging sources of OVOC emissions, such as ancillary solvent use associated with vehicles, are not yet incorporated into emission estimation methodologies (Cliff et al., 2023). Collectively, uncertainties in emissions and chemical mechanisms contribute to substantial underestimations of certain OVOCs, such as HCHO, alcohols, ketones, and organic acids, particularly in urban environments dominated by anthropogenic emissions (Luecken et al., 2018; He et al., 2024; Liu et al., 2023; Pfannerstill et al., 2023). In recent years, several studies have developed OVOC emission profiles with improved speciation and quantification accuracy (Wang et al., 2024a; Wang et al., 2022a; Ou et al., 2015; Mo et al., 2016). Nevertheless, differences in emission development methods and the limited representation of source categories lead to substantial variations in reported OVOC and VOC source profiles (Niu et al., 2023), which hinder systematic investigations into the spatiotemporal characteristics of OVOCs and their roles in regional ozone formation.

In this study, an updated emission inventory with refined profiles of OVOCs and their VOC precursors was incorporated into the Community Multiscale Air Quality (CMAQ) model to improve and evaluate OVOC simulations over the Yangtze River Delta (YRD) region in China. Our previous work demonstrates the critical role of OVOC oxidation in enhancing atmospheric oxidation capacity and promoting ozone formation in this region, based on top-down emission adjustments constrained by field observations (Li et al., 2022a). Here, we adopt a process-oriented approach by integrating sector-specific source profiles into the emission inventory to quantify the contributions of primary emissions to ambient OVOC levels in the YRD. We further investigate the respective roles of emitted and secondary OVOCs in ozone and HO₂ production. A subsequent sensitivity analysis is conducted to assess the relative impacts of emitted OVOCs and traditional VOC precursors on ozone mitigation during a pollution episode. These findings advance our understanding of OVOC fate in the atmosphere and their impact on urban ozone chemistry.





2 Methodology

95

100

105

110

2.1 Model description

The CMAO model version 5.2, coupled with the SAPRC07tic chemical mechanism and the AERO6 aerosol module, was applied to simulate OVOC distributions in the YRD during March 27-April 30 (EP1) and October 15-November 20 (EP2) of 2019. Several model updates, including heterogeneous reactions of sulfur dioxide (SO2), NO2, glyoxal, and methylglyoxal, were implemented as described in a previous study (Mao et al., 2022). Two nested domains were configured, with the outer domain (d01) covering eastern China and the inner domain (d02) encompassing the YRD. These domains had horizontal resolutions of 12 km × 12 km (127 × 202 grid cells) and 4 km × 4 km (238×268 grid cells), respectively (Fig. S1). Meteorological fields were generated using the Weather Research and Forecasting (WRF) model version 4.2.2, with initial and boundary conditions provided by the fifth generation ECMWF atmospheric reanalysis of the global climate (ERA5). Anthropogenic emissions in d01 were derived from the Multi-resolution Emission Inventory for China (MEIC) version 1.4 (Geng et al., 2024) for mainland China and the Regional Emission inventory in ASia (REAS) version 3.2.1 (Kurokawa and Ohara, 2020) for other Asian countries and regions. For d02, the 2019 YRD emission inventory incorporating updated VOC profiles (2019 YRD inventory) was applied to the YRD, while the MEICv1.4 was used for the remaining regions. Biogenic emissions were generated using the Model of Emissions of Gases and Aerosols from Nature (MEGAN) version 2.1. Open biomass burning emissions were based on the Fire INventory from NCAR (FINN) version 2.5 (Wiedinmyer et al., 2023). The spatial and temporal allocations of anthropogenic and open biomass burning emissions followed previous work (Hu et al., 2016; An et al., 2021). Notably, the temporal allocation did not account for temporary emission control measures, which may partly explain the model biases discussed later. The first five days of each simulation were treated as spin-up and excluded from the analysis. A complete list of all OVOCs and their precursors used in the model is provided in Table S1. The 2019 YRD inventory was developed based on the 2017 version (An et al., 2021), with updated activity data for each source sector. Key improvements included refined VOC speciation, particularly of OVOCs, for major source categories such as transportation (gasoline and diesel vehicles), industrial processes, and residential biomass burning (Gao et al., 2022; Wang et al., 2022a). The chemical composition of VOCs from diesel vehicles, industrial processes, and biomass burning was characterized

115

120

130

135

140





based on 160 localized, source-resolved measurements conducted in China. Details of the sampling and analytical procedures can be found in our previous study (Gao et al., 2023). VOC profiles for other sources, such as gasoline vehicles, were updated based on published literature (Wang et al., 2022a; Huang et al., 2024).

As a result of these refinements, OVOCs accounted for 56.8% of total VOC emissions from diesel vehicles (DVE), followed by 44.6% from residential biomass burning (RBB) and 39.1% from industrial processes (INP) (Table S2). Among all OVOCs, carbonyl species showed significant enhancements in these three source categories. Aldehyde contributions nearly doubled in DVE and INP, with a particularly large increase in HCHO. In contrast, the emissions of alcohols, such as methanol (MEOH) and ethanol (ETOH) from INP, decreased. Contributions from other OVOCs, including acetic acid (CCOOH) as well as phenols and cresols (CRES), also increased in INP and DVE. Although the overall OVOC fraction from gasoline vehicle emissions slightly decreased, the chemical composition exhibited a marked change, with increases in carbonyls and decreases in alcohols and esters.

125 **2.2 Observation data**

A suite of pollutant and meteorological observations from ground monitoring stations (Fig. S1) was collected for model evaluation. High time-resolution measurements of 77 OVOCs, including 14 aldehydes and ketones, 23 organic acids and esters, 10 furan compounds, and 30 oxygenated aromatic compounds, were recorded at a 10 s interval using a Proton Transfer Reaction-Quadruple interface Time-of-Flight Mass Spectrometer (PTR-QiTOF) at the Shanghai Academy of Environmental Sciences. After removing outliers (values below the background level) and missing data, the remaining data were averaged to hourly means. In addition, C₂–C₁₂ hydrocarbons, C₂–C₅ carbonyls, and C₁–C₄ alcohols were measured using an online gas chromatography system equipped with a mass spectrometer and a flame ionization detector (GC-MS/FID, TH-300, Wuhan Tianhong Instruments, China) at an hourly resolution. Formaldehyde and peroxyacetyl nitrate (PAN) were measured using a commercial Hantzsch fluorimetry monitor and an online gas chromatography-electron capture detector (GC-ECD), respectively. Details on the instrumentation, analytical procedures, and data quality assurance have been described in previous work (Gao et al., 2022; Liu et al., 2019; Du et al., 2025).

Hourly O₃ concentrations in 14 cities across the YRD were obtained from the China National

145

150

155

160

165





Meteorological parameters, including temperature, relative humidity, wind speed, and wind direction, were obtained for four representative cities (Shanghai, Nanjing, Hefei, and Hangzhou) from the China Meteorological Administration (http://data.cma.cn/; last access: 1 November 2024). To evaluate model performance, statistical metrics such as Pearson correlation coefficient (R), mean bias (MB), mean error (ME), normalized mean bias (NMB), normalized mean error (NME), root mean square error (RMSE), and index of agreement (IOA) were calculated and compared against benchmark values where available. Additional details are provided in Text S1.

3 Results and Discussion

3.1 Characteristics of OVOCs

Among all the observed OVOCs, alcohols were the dominant species in spring (EP1), with ethanol exhibiting the highest hourly median concentrations, ranging from 6 to 12 ppb, which dropped to below 0.5 ppb in fall (EP2) (Figs. 1 and S6). The model exhibited opposite biases, underestimating ethanol in EP1 while overestimating it in EP2. This discrepancy may be attributed to uncertainties in the emission inventory. The monitoring site is located in a typical urban environment surrounded by commercial and residential buildings and busy roads, where emissions from transportation and solvent use have a strong influence (Liu et al., 2019; Liu et al., 2021). One likely underestimated source of alcohols is the use of alcohol-containing solvent products such as windshield washer fluid, particularly from electric vehicles (Cliff et al., 2023). Considering the rapid growth in electric vehicle ownership in China in recent years, this alcohol source will likely become more important. Another potential source of alcohols is the use of household cleaning and personal care products, which may not be fully represented in the current emission inventory (Mo et al., 2021; Wang et al., 2024b). In contrast, the overestimation in EP2 may result from the model's omission of temporary emission restrictions implemented in the period before and during the China International Import Expo 2019 (CIIE 2019, October 27-November 10, 2019) (Wang et al., 2025). Observational data show that ethanol concentrations remained extremely low (< 0.5 ppb) before November 12, but rebounded to 2-15 ppb thereafter, reaching levels comparable to those during EP1 (Fig. S7). Additionally, a major source of ethanol in the current inventory is solvent use (e.g., paints, coatings, adhesives, etc.), which is estimated based on solvent consumption and chemical composition without incorporating temperature-dependent parameterization (An et al., 2021). The





opposite model biases between the two episodes may be partially attributed to the inadequate treatment 170 of temperature-dependent evaporative emissions (Qin et al., 2025), given ethanol's high volatility and the 2.5°C (16.8%) higher average temperature in EP1 compared to EP2 (Fig. S8). Formic acid and acetic acid were the most abundant organic acids during both episodes, but were consistently underestimated by the model, with larger biases in EP2 (Fig. S6 and Table S5). These discrepancies may be partially attributed to uncertainties in the emission inventory. Acetic acid showed 175 strong correlations with ethyl acetate, methyl ethyl ketone (MEK), and toluene (Pearson coefficients of 0.75-0.85, p < 0.001) in both periods. These species are often associated with volatile chemical product (VCP) emissions (Wang et al., 2024b; McDonald et al., 2018), which are likely underestimated in the current model. However, MEK and toluene may also originate from other sources, such as fuel combustion, and their model performance varied between episodes—being slightly underestimated in 180 EP1 but overestimated in EP2, likely due to the absence of short-term emission controls in the model during CIIE 2019. In addition to primary emissions, the underestimation of both acids may also be attributed to insufficient secondary production. For example, formic acid showed a moderate to strong correlation with its precursor methylglyoxal, yet both were significantly underestimated. Further discrepancies may result from missing secondary formation pathways and underestimated yields of 185 formic and acetic acids from precursor VOCs (Yuan et al., 2015; Millet et al., 2015; Permar et al., 2023). Most carbonyl species were well captured by the model. During the warm season (EP1), observed carbonyl concentrations exhibited pronounced diurnal variations with daytime maxima, primarily driven by photochemical production. In contrast, such diurnal patterns were less evident in EP2 (Fig. S6), likely due to reduced secondary formation under lower atmospheric oxidation capacity (Fig. S9). HCHO and 190 acetone (ACET) were the most abundant aldehyde and ketone species, respectively. HCHO is a common oxidation product of VOCs in the troposphere and can also originate from primary emissions, including fuel and biomass combustion, industrial processes, and the evaporation of indoor building materials (Wang et al., 2022a; Xing et al., 2024; Liang and Yang, 2013; Permar et al., 2021). The model generally reproduced the observed HCHO concentrations, although slight underestimations persisted in both 195 seasons (Table S5). Model performance for ACET varied seasonally, with good agreement in EP2 but significant underestimation in EP1. Given acetone's high volatility and substantial emissions from solvent use (Stockwell et al., 2021; Lewis et al., 2020), the bias in EP1 may partially result from uncertainties in the temperature-dependent emission estimation in the current inventory. Additionally,

200

205

210

215

220





since biogenic sources of acetone are important (Lyu et al., 2024; Hu et al., 2013), the larger discrepancy observed in the warm season may also be due to the model's inadequate representation of urban green vegetation (Maison et al., 2024; Ma et al., 2022).

Notably, biases in OVOC concentrations are influenced by those of their precursors. For example, model biases in methacrolein (MACR) and methyl vinyl ketone (MVK) exhibited similar temporal patterns to those of isoprene (ISOP), reflecting their common origin via isoprene oxidation. The model reasonably reproduced key OVOC precursors, including reactive alkanes (ALK3/ALK4), aromatic hydrocarbons, and alkenes (e.g., ethylene and propylene), particularly during EP1. This suggests that biases related to secondary OVOC production were less pronounced in EP1 than in EP2, consistent with the larger discrepancies observed in EP2 (Table S5). The simultaneous overestimation of VOC precursors and underestimation of OVOCs also indicates that uncertainties in their photochemical mechanisms may contribute to the model biases in OVOC concentrations.

At the regional scale, average OVOC concentrations across the YRD ranged from 5 to 25 ppb in both seasons, with elevated levels observed in the central and eastern areas (Figs. 2a and 2d). HCHO, MEOH, ACET, and acetaldehyde (CCHO) were the dominant species (Fig. S10). Most OVOCs exhibited higher concentrations in EP2 than in EP1, except for MEOH, likely due to its stronger biogenic contribution during the warm season, particularly in the southern and southwestern YRD. On average, the model predicted that approximately 30–70% of total OVOCs originated from primary emissions (primary OVOCs) rather than from VOC oxidation (secondary OVOCs). The contributions of primary OVOCs show significant seasonal and spatial variations. During the warm season, secondary OVOCs dominated across the entire domain, while elevated emission contributions were observed in hotspots along the Yangtze River and in Shanghai (Fig. 2b). In contrast, during the cold season, primary OVOCs played a larger role in Jiangsu Province as well as in Shanghai and Hangzhou (Fig. 2e), consistent with our previous findings for October 2017 in the YRD(Li et al., 2022a).

230





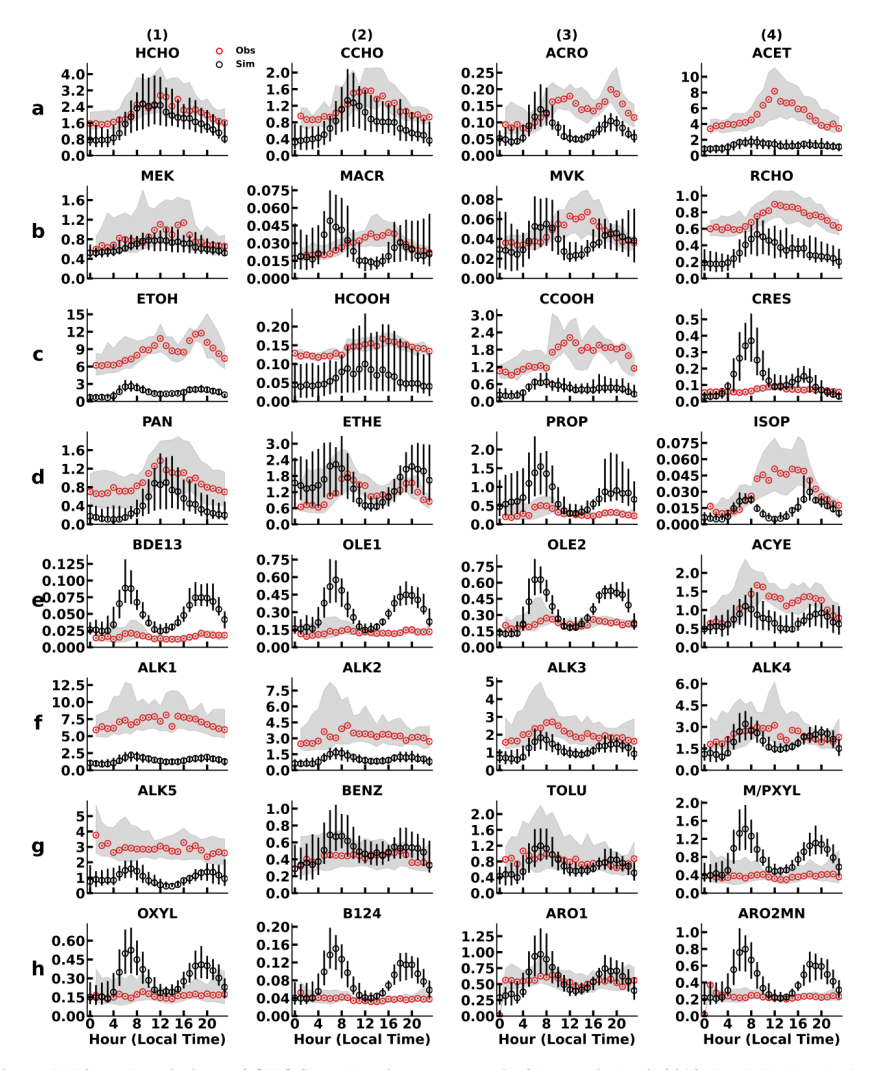


Figure 1. Diurnal variations of OVOCs and their precursors in Shanghai, April 2019 (ppb). Red and black circles indicate the median observations and model predictions, respectively; shaded areas and black error bars represent the interquartile ranges (25th-75th percentiles) of observations and model predictions, respectively.

CRES accounted for the highest OVOC emission rate across the YRD (22%), followed by HCHO (16%), ACET (14.5%), CCOOH (12.5%), and ETOH (9.5%) (Table S6). High emission contributions to ambient CRES and CCOOH were also observed, followed by ACET (Fig. S11). Primary emissions accounted for approximately 20–60% of ambient HCHO, with maxima reaching up to 76% in EP1 and 88% in EP2 in Jiangsu Province. The model also estimated a substantial fraction of biacetyl (BACL) originating from primary emissions (more than 60%), particularly in Jiangsu and Anhui Provinces, as well as Shanghai.





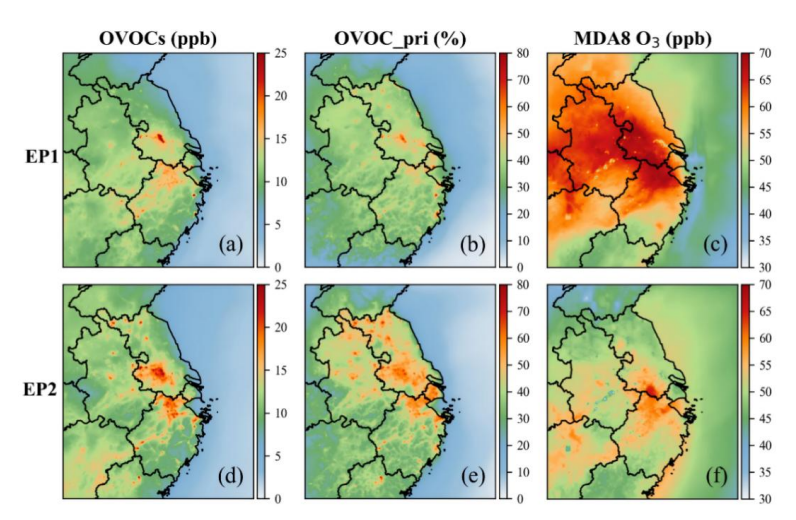


Figure 2. Episode-averaged total OVOC concentrations (a, d), primary emission contributions to total OVOCs (b, e), and daily maximum 8-hour average ozone (MDA8 O₃) concentrations (c, f) during the two episodes.

The spatial distributions of OVOCs and ozone were closely aligned, with OVOC hotspots coinciding with regions of elevated daily maximum 8-hour average ozone (MDA8 O₃) concentrations (Figs. 2c and 2f). Further analysis revealed that OVOC photooxidation constituted a significant source of HO₂ radicals in the YRD, serving as a key driver of NO-NO₂ cycling and thereby influencing ozone formation.

3.2 Role of OVOCs in Ozone Formation

240

245

250

To investigate the relationship between OVOCs and O_3 formation at the monitoring site in Shanghai, a "clean period" (April 1–4) and a "pollution period" (April 5–7) were selected. During the clean period, observed MDA8 O_3 concentrations (81.4–139.4 μ g/m³) complied with China's Ambient Air Quality Standards (GB 3095-2012) threshold of 160 μ g/m³. In contrast, MDA8 O_3 levels during the pollution period ranged from 161.3 μ g/m³ to 189.1 μ g/m³, exceeding this standard. The model showed good agreement with observations, successfully capturing temporal variations of both MDA8 O_3 and OVOC concentrations during these periods, demonstrating its capability to represent OVOC sources and sinks as well as their role in ozone formation.

The ozone production rate $(P(O_3), ppb/h)$, defined as the rate at which ozone is produced through the conversion of NO to NO₂ by peroxy radicals, was calculated as follows:

$$P(O_3) = k_0[HO_2][NO] + \sum_i k_i [RO_2^i][NO],$$
 (1)





where k₀ and k_i are the rate constants for the reactions of NO with HO₂ and RO₂ radicals (unit: molec⁻¹ cm³ s⁻¹), respectively, and [HO₂], [RO₂], and [NO] denote their respective concentrations (unit: ppb). In 255 RO₂ + NO reactions, alkyl nitrates can form as byproducts, with yields (α) depending on the specific RO₂ species. Accordingly, a NO₂ yield of (1-α) was applied to the corresponding RO₂ + NO reactions. The NO₂ molar yields for reactions producing alkyl nitrate coproducts in the current model are listed in Table S7. The analysis of P(O₃) and radical chemistry is focused on the daytime period (9:00 - 17:00 local time). As shown in Figs. 3a and 3b, the daytime average P(O₃) during the clean period was approximately half 260 that under the polluted conditions, at 5.89 ppb/h and 12.2 ppb/h, respectively. HO₂-driven oxidation accounted for 51-59% of daytime P(O₃) during the clean period, increasing slightly to 50-61% under the polluted conditions. Ozone production via the HO₂ pathway peaked around noon, coinciding with the highest P(O₃), and declined gradually to approximately 50% later in the day. These results indicate that 265 the HO₂ pathway consistently dominates ozone production in Shanghai, regardless of pollution levels. The dominant role of HO₂-driven oxidation in ozone production was further confirmed in other urban areas of the YRD. During both EP1 and EP2, HO2 radicals contributed approximately 55-80% of total ozone production in regions with elevated P(O₃) (Figs. 4 and S12). These areas, including Shanghai, are heavily influenced by anthropogenic emissions, where HO2 concentrations exceeded those of RO2 270 radicals (Fig. S12). In contrast, RO2 radicals dominated ozone production in the southern and southwestern parts of the domain, where high biogenic VOC emissions and relatively low NOx levels prevail. The enhanced role of RO2 radicals in these regions is attributed to their higher concentrations and comparable reactivities to HO2 radicals in converting NO to NO2. To understand the mechanism of daytime HO2 radical production, source contributions from the primary HO₂ generated by OVOCs and VOCs, RO₂ reactions, and other pathways of inorganic species in Shanghai were investigated (Fig. 3c). It should be noted that HO₂ produced directly during OVOC and VOC oxidation, excluding formation via RO2 chain reactions, is defined as "primary" HO2, whereas HO2 formed through reactions without radical reactants, such as photolysis and O₃-initiated reactions, is referred to as "newly generated" HO2. The contribution of HNO4 was excluded, as NO2 and HO2 can 280 react rapidly to reproduce HNO₄. Under the clean conditions, the primary HO₂ production through VOC and OVOC photooxidation dominated among all pathways, accounting for 30.3% and 29.9% of the total, respectively. Reactions involving inorganic species, such as CO + OH, accounted for approximately 22.0%

290

295

300





of total HO_2 production. Another important source was the reactions of RO_2 with NO and RO_2 radicals (17.9%), with the RO_2 + NO pathway being dominant. In the HO_2 pool, approximately 16.6% was newly generated, with OVOC photolysis being the dominant source (94.1%). Similar findings have been reported in other urban areas, where OVOC photolysis accounted for over 80% of newly generated HO_2 radicals, highlighting its importance in NO_x cycling and ozone production(Qu et al., 2021; Xue et al., 2016; Yang et al., 2018).

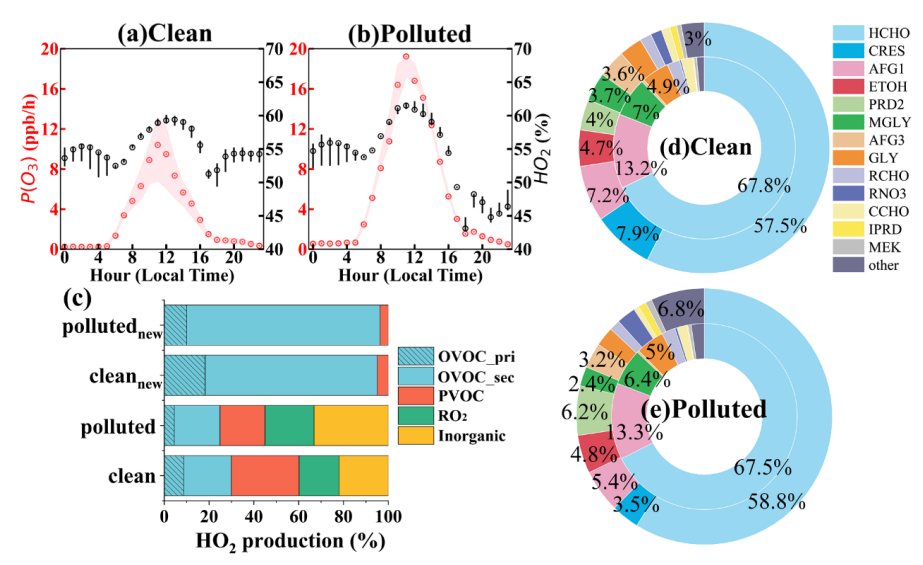


Figure 3. Diurnal variations of ozone production rate (a, b) and source contributions to daytime HO₂ production (c-e) under clean and polluted conditions in Shanghai. In panels (a) and (b), red and black circles represent the median P(O₃) and the contribution of the HO₂ + NO pathway, respectively. The shaded areas and black error bars denote the interquartile ranges. In panel (c), "PVOC" denotes primary HO₂ production from VOC precursors of OVOCs, while "OVOC_pri" and "OVOC_sec" denote primary HO₂ production from emitted and secondary generated OVOCs, respectively. "polluted_{new}" ("clean_{new}") and "polluted" ("clean") refer to newly generated HO₂ and the total HO₂ production, respectively, under the polluted (clean) conditions. Panels (d) and (e) show the fractional contributions of individual OVOCs to total (outer circle) and newly generated (inner circle) primary HO₂ production.

Under the polluted conditions, contributions from inorganic species increased to about one-third of the total HO₂ production, mainly due to elevated CO levels. The primary HO₂ generated by OVOC oxidation became the largest organic source (24.9%), followed by the RO₂ pathway (21.9%). In addition, the fraction of newly generated HO₂ decreased to 9.86%, suggesting an enhanced radical propagation effect and higher atmospheric oxidation capacity under the polluted conditions. As a result, the contribution of

310

315

320

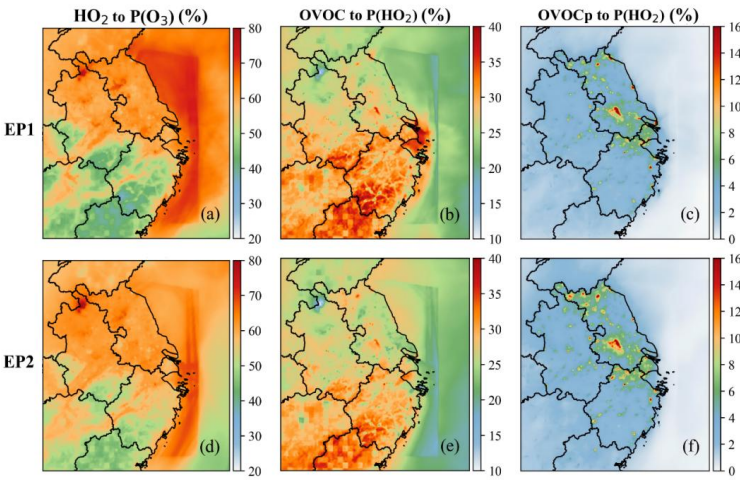




secondary-generated OVOCs to their total primary HO₂ production rose from 71% to 82%. Overall, OVOC photooxidation plays an important role in the HO₂ production across pollution conditions.

Among all OVOCs, HCHO was the most significant contributor to HO₂ (~60%) under both clean and polluted conditions. Under the clean conditions, CRES was the second-largest contributor, followed by photoreactive monounsaturated dicarbonyls from aromatic fragmentation (AFG1) and ethanol. Under the polluted conditions, reactive ketones (PRD2) became the second-largest contributor, followed by AFG1. These species were mainly produced from VOC oxidation. For newly generated HO₂ radicals, glyoxal and methylglyoxal also contributed substantially. These findings align with a modeling study in Beijing, which showed that HCHO, MGLY, and aromatic oxidation products played an important role in HO₂ production(Qu et al., 2021).

Across the YRD, primary HO₂ produced by OVOC oxidation contributed 20–40% of the total HO₂ when the HNO₄ pathway was excluded (Figs. 4b and 4e), exceeding contributions from both VOC precursor oxidation and the RO₂ pathway (Fig. S13). Due to high CO emissions, the CO + OH reaction accounted for 20–50% of the total HO₂ production, with a more pronounced contribution in the northern YRD (Figs. S13c and S13f). OVOC photolysis can become the dominant source of the newly generated HO₂ radicals, contributing up to 98% regionally. Primary emitted OVOCs made substantial contributions to HO₂ production in Jiangsu Province, particularly near Zhenjiang and northern Jiangsu, as well as in Shanghai and Huzhou (Figs. 4c and 4f). Among the total and newly generated primary HO₂ from OVOC oxidation, emitted OVOCs contributed 15–40% and 10–25% (Fig. S14), respectively, highlighting their important role in driving ozone production in the YRD.



335

340

345

350





Figure 4. Daytime-averaged contributions of the HO₂ + NO pathway to ozone production rates (a, d), contributions of primary HO₂ production from OVOC to total HO₂ radical production (b, e), and contributions from emitted OVOCs (c, f) during the two episodes.

3.3 Sensitivity of Ozone Formation to OVOCs and Precursors

Given that a substantial fraction of OVOCs originates from primary emissions, the sensitivity of ozone formation to anthropogenic emissions of OVOCs and their precursors was systematically examined using the CMAQ model coupled with the High-Order Decoupled Direct Method (HDDM). The model configuration followed Li et al(Li et al., 2022b), with the same inputs described in Section 2.1. The ozone responses to the complete removal of various VOCs (Δ O₃) in Shanghai, along with their normalized contributions relative to total anthropogenic emissions across the domain (Δ O₃/ Δ E_i) under different polluted conditions, are discussed below.

ppb and 1.01 ppb to ozone formation under clean and polluted conditions, respectively (Fig. 5a). These ozone changes were comparable to those of most VOC precursors except ETHE. BACL was also a key OVOC precursor, contributing 0.35 ppb and 0.50 ppb of ozone under clean and polluted conditions, respectively. BACL undergoes photolysis to produce acetyl peroxy radicals (CH₃CO₃), which facilitate NO-to-NO₂ conversion at a rate significantly higher than most other peroxy radicals represented in the model. On a per-unit-mass basis, OVOCs demonstrated substantially higher ozone formation efficiencies than other VOC precursors. Notably, BACL emerged as the most potential contributor in Shanghai, generating 7.78×10^{-4} ppb and 1.49×10^{-3} ppb of ozone per gram emitted under clean and polluted conditions, respectively. HCHO, MVK, MACR, and MGLY also exhibited relatively high ozone formation efficiencies, contributing $(1.57-3.77) \times 10^{-4}$ ppb per gram emitted across both conditions. Similar sensitivities of O₃ formation to OVOC and VOC precursor emission controls were also observed across the YRD. Among all OVOCs, HCHO demonstrated the most pronounced impact, with emission reductions leading to ozone decreases of up to 2.0 ppb in Jiangsu Province (Fig. S15). This effect was comparable to that of aromatic hydrocarbons (ARO2MN and TOLU) and reactive alkenes (OLE2), and exceeded the influence of most other VOC precursors, except ETHE and propylene (PROP). BACL also exhibited considerable effects, causing up to 1.0 ppb decreases in O₃, similar to reactive alkanes (ALK3-5), alkenes (OLE1), and most aromatic hydrocarbons. Notably, not all OVOC emission reductions yielded effective ozone mitigation; certain compounds, such as CCHO and CRES, exhibited nonlinear





responses. In some cases, reducing their emissions slightly increased ozone concentrations, likely due to complex interactions with other reactive species. Nonetheless, controlling emissions of OVOCs, particularly HCHO and BACL, represents an efficient strategy for reducing O₃ in the YRD.

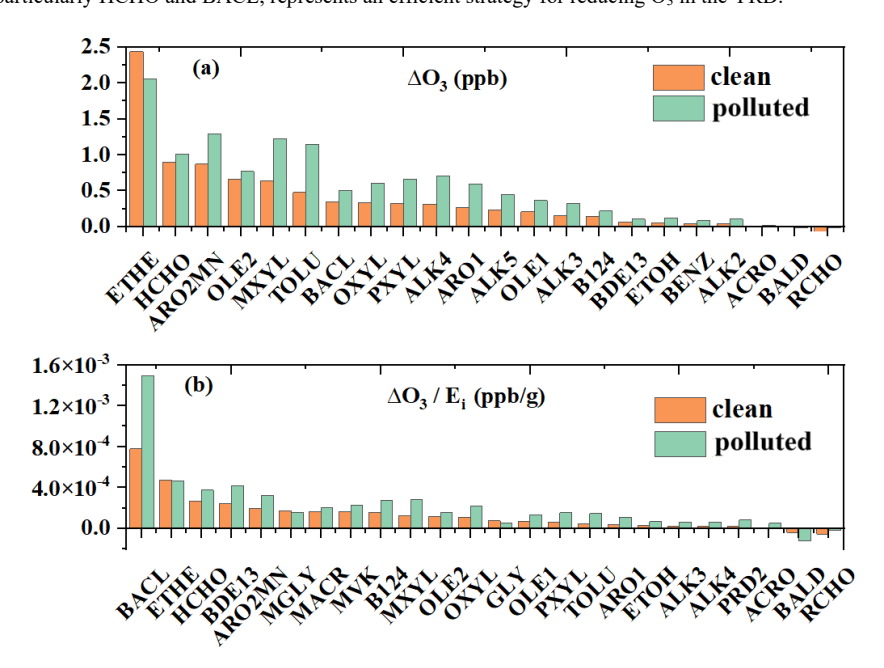


Figure 5. Sensitivity of daytime average ozone to individual OVOCs and VOC precursors (a), and emission-normalized ozone changes (b) in Shanghai during the clean and polluted periods.

4 Conclusions

360

365

370

OVOCs are key precursors of peroxy radicals that drive NO-to-NO₂ conversion, thereby facilitating O₃ accumulation in the troposphere. Model biases in simulating OVOCs are often attributed to uncertainties in VOC precursor emissions and the photochemical mechanisms used in chemical transport models. However, we emphasize that primary anthropogenic emissions constitute significant yet often underrepresented sources of ambient OVOCs, particularly in urban environments where industrial activities, solvent use, and fuel combustion dominate. High local emission contributions to ambient OVOCs (9–53% for carbonyl compounds and 50–87% for alcohols) have also been reported in other Chinese cities based on field measurements (Wu et al., 2020; Huang et al., 2020). Certain OVOCs, such as formaldehyde, acetone, and alcohols, are highly volatile, and their emission rates are therefore expected to exhibit strong temperature dependence. This inference is supported by direct measurements

375

380

385

390

395

400





significantly higher proportions of OVOCs in total VOC emissions from car painting, waste transfer station, and laundry sources in summer than in winter (Niu et al., 2021). With ongoing climate warming and more frequent heatwave events, emissions of these OVOC species are expected to increase, potentially enhancing atmospheric oxidation capacity and accelerating secondary pollutant formation. The impacts of such temperature-driven increases in OVOC emissions remain insufficiently understood. HO₂ radicals dominated ozone formation in urban areas of the YRD, contributing 50-60% of the daytime ozone production rate under both clean and polluted conditions in Shanghai, and ranging from 55% to 80% across the region during both warm and cold seasons. This is consistent with findings from other urban environments heavily influenced by anthropogenic emissions (Zhu et al., 2024; Tan et al., 2019a; Hu et al., 2023). Therefore, emission controls targeting major HO₂ radical contributors could be an effective strategy for ozone mitigation in urban regions like the YRD. Traditionally, the significance of OVOCs in the free radical budget has been mainly recognized through their formation as secondary products from VOC precursors. However, we demonstrated that primary HO2 produced via OVOC photooxidation accounted for 20-40% of total HO₂ production, with 15-40% of this attributed to emitted OVOCs. As a result, key OVOC species (e.g., HCHO) can compete with their precursors in generating HO₂ radicals and influence ozone formation. In addition, the contributions of OVOCs to RO₂ radicals, such as BACL, also promote ozone production and should not be overlooked. Several uncertainties remain in the current study. Improvements are needed in representing multiphase chemistry, especially in detailed VOC speciation, multistep oxidation reactions, and the heterogeneous production and/or loss of small aldehydes and carboxylic acids. Additionally, emission profiles of organic acids and alcohols require further refinement, along with improved characterization of the temperature dependence of evaporative emissions. Previous studies have shown that alcohols contribute substantially to total OH reactivity and ozone formation, with their impacts intensifying at higher temperatures (Pfannerstill et al., 2023; Luecken et al., 2018; Pusede et al., 2014); however, large discrepancies between modeled and observed concentrations of these compounds were identified in the current study. Moreover, limited observational data confined the analysis to spring and fall. Future studies should extend to all seasons and other regions, focusing on OVOC emission contributions to ambient levels and the sensitivity of ozone formation to OVOC emission reductions, with improved representation of OVOC emissions, speciation, and multiphase chemistry.

of 13 volatile emission sources during a sampling campaign in central China, which revealed

https://doi.org/10.5194/egusphere-2025-4919 Preprint. Discussion started: 13 November 2025

© Author(s) 2025. CC BY 4.0 License.



EGUsphere Preprint repository

Code and data availability

The CMAQ source code can be downloaded at https://github.com/USEPA/CMAQ. The input files to

CMAQ, WRF, and MEGAN, and meteorology and ozone observation data can be downloaded from the

405 links and cited references given in the methods section. VOC observation data at Shanghai and Python

scripts for processing data and generating figures are available upon reasonable request from the

corresponding author.

Author contributions

J.L. designed the research. X.L. and X.L. conducted the simulations and analyzed the data. R.Y., Y.G.,

410 and H.W. provided the 2019YRD emissions and ground observation data of VOCs at Shanghai. X.L.

drafted the main text. All authors contributed to interpreting the results and editing the manuscript.

Competing interests

The authors declare that they have no conflict of interest.

Acknowledgements

415 This work was financially supported by the National Key R&D Program of China (grant no.

2022YFE0136200; 2023YFC3706105) and the National Natural Science Foundation of China (grant no.

42077199).

References

420 An, J., Huang, Y., Huang, C., Wang, X., Yan, R., Wang, Q., Wang, H., Jing, S., Zhang, Y., Liu, Y., Chen,

Y., Xu, C., Qiao, L., Zhou, M., Zhu, S., Hu, Q., Lu, J., and Chen, C.: Emission inventory of air pollutants

and chemical speciation for specific anthropogenic sources based on local measurements in the Yangtze

River Delta region, China, Atmos. Chem. Phys., 21, 2003-2025, 10.5194/acp-21-2003-2021, 2021.

17





- Cliff, S. J., Lewis, A. C., Shaw, M. D., Lee, J. D., Flynn, M., Andrews, S. J., Hopkins, J. R., Purvis, R.
- 425 M., and Yeoman, A. M.: Unreported VOC Emissions from Road Transport Including from Electric Vehicles, Environ. Sci. Technol., 57, 8026-8034, 10.1021/acs.est.3c00845, 2023.
 - Du, C., Wang, H., Gao, Y., Yan, R., Jing, S. a., Zhou, M., Wang, Q., Lou, S., Huang, C., Huang, D. D., Shang, Y., and An, J.: Processes Driving Diurnal and Seasonal Variations of Formaldehyde in an Urban Environment, ACS Earth Space Chem., 9, 1174-1184, 10.1021/acsearthspacechem.5c00020, 2025.
- Gao, Y., Wang, H., Yuan, L., Jing, S., Yuan, B., Shen, G., Zhu, L., Koss, A., Li, Y., Wang, Q., Huang,
 D. D., Zhu, S., Tao, S., Lou, S., and Huang, C.: Measurement report: Underestimated reactive organic gases from residential combustion insights from a near-complete speciation, Atmos. Chem. Phys., 23, 6633-6646, 10.5194/acp-23-6633-2023, 2023.
 - Gao, Y. Q., Wang, H. L., Liu, Y., Zhang, X., Jing, S. A., Peng, Y. R., Huang, D. D., Li, X., Chen, S. Y.,
- 435 Lou, S. R., Li, Y. J., and Huang, C.: Unexpected High Contribution of Residential Biomass Burning to Non-Methane Organic Gases (NMOGs) in the Yangtze River Delta Region of China, J. Geophys. Res. Atmos., 127, 14, 10.1029/2021jd035050, 2022.
 - Geng, G., Liu, Y., Liu, Y., Liu, S., Cheng, J., Yan, L., Wu, N., Hu, H., Tong, D., Zheng, B., Yin, Z., He, K., and Zhang, Q.: Efficacy of China's clean air actions to tackle PM2.5 pollution between 2013 and
- 440 2020, Nat. Geosci, 17, 987-994, 10.1038/s41561-024-01540-z, 2024.
 - Gkatzelis, G. I., Papanastasiou, D. K., Karydis, V. A., Hohaus, T., Liu, Y., Schmitt, S. H., Schlag, P., Fuchs, H., Novelli, A., Chen, Q., Cheng, X., Broch, S., Dong, H., Holland, F., Li, X., Liu, Y., Ma, X., Reimer, D., Rohrer, F., Shao, M., Tan, Z., Taraborrelli, D., Tillmann, R., Wang, H., Wang, Y., Wu, Y., Wu, Z., Zeng, L., Zheng, J., Hu, M., Lu, K., Hofzumahaus, A., Zhang, Y., Wahner, A., and Kiendler-
- Scharr, A.: Uptake of Water-soluble Gas-phase Oxidation Products Drives Organic Particulate Pollution in Beijing, Geophys. Res. Lett., 48, e2020GL091351, https://doi.org/10.1029/2020GL091351, 2021.
 He, M., Ditto, J. C., Gardner, L., Machesky, J., Hass-Mitchell, T. N., Chen, C., Khare, P., Sahin, B., Fortner, J. D., Plata, D. L., Drollette, B. D., Hayden, K. L., Wentzell, J. J. B., Mittermeier, R. L., Leithead, A., Lee, P., Darlington, A., Wren, S. N., Zhang, J., Wolde, M., Moussa, S. G., Li, S.-M., Liggio, J., and
- Gentner, D. R.: Total organic carbon measurements reveal major gaps in petrochemical emissions reporting, Science, 383, 426-432, 10.1126/science.adj6233, 2024.
 - Hu, B. Y., Chen, G. J., Chen, J. S., Xu, L. L., Fan, X. L., Hong, Y. W., Li, M. R., Lin, Z. Y., Huang, M. Q., Zhang, F. W., and Wang, H.: The effect of nitrous acid (HONO) on ozone formation during pollution





- episodes in southeastern China: Results from model improvement and mechanism insights, Sci. Total
- 455 Environ., 891, 13, 10.1016/j.scitotenv.2023.164477, 2023.
 - Hu, J., Chen, J., Ying, Q., and Zhang, H.: One-year simulation of ozone and particulate matter in China using WRF/CMAQ modeling system, Atmos. Chem. Phys., 16, 10333-10350, 10.5194/acp-16-10333-2016, 2016.
 - Hu, L., Chen, L., Lin, W., Yao, L., Feng, Y., Zhao, J., Wu, W., Zheng, C., and Gao, X.: Quantifying
- 460 Real-Time VOC Emissions of Typical Sources in the Chemical Industrial Park Using Multiplexed Online Mass Spectrometry, Environ. Sci. Technol., 59, 22784-22795, 10.1021/acs.est.5c11270, 2025.
 - Hu, L., Millet, D. B., Kim, S. Y., Wells, K. C., Griffis, T. J., Fischer, E. V., Helmig, D., Hueber, J., and Curtis, A. J.: North American acetone sources determined from tall tower measurements and inverse modeling, Atmos. Chem. Phys., 13, 3379-3392, 10.5194/acp-13-3379-2013, 2013.
- Huang, D. D., Hu, Q., He, X., Huang, R.-J., Ding, X., Ma, Y., Feng, X., Jing, S. a., Li, Y., Lu, J., Gao, Y., Chang, Y., Shi, X., Qian, C., Yan, C., Lou, S., Wang, H., and Huang, C.: Obscured Contribution of Oxygenated Intermediate-Volatility Organic Compounds to Secondary Organic Aerosol Formation from Gasoline Vehicle Emissions, Environ. Sci. Technol., 58, 10652-10663, 10.1021/acs.est.3c08536, 2024. Huang, X.-F., Zhang, B., Xia, S.-Y., Han, Y., Wang, C., Yu, G.-H., and Feng, N.: Sources of oxygenated
- volatile organic compounds (OVOCs) in urban atmospheres in North and South China, Environ. Pollut., 261, 114152, https://doi.org/10.1016/j.envpol.2020.114152, 2020.
 - Kurokawa, J. and Ohara, T.: Long-term historical trends in air pollutant emissions in Asia: Regional Emission inventory in ASia (REAS) version 3, Atmos. Chem. Phys., 20, 12761-12793, 10.5194/acp-20-12761-2020, 2020.
- Lewis, A. C., Hopkins, J. R., Carslaw, D. C., Hamilton, J. F., Nelson, B. S., Stewart, G., Dernie, J., Passant, N., and Murrells, T.: An increasing role for solvent emissions and implications for future measurements of volatile organic compounds, Phil. Trans. R. Soc. A., 378, 20190328, doi:10.1098/rsta.2019.0328, 2020.
 - Li, J. Y., Xie, X. D., Li, L., Wang, X. Y., Wang, H. L., Jing, S. A., Ying, Q., Qin, M. M., and Hu, J. L.:
- Fate of Oxygenated Volatile Organic Compounds in the Yangtze River Delta Region: Source Contributions and Impacts on the Atmospheric Oxidation Capacity, Environ. Sci. Technol., 56, 11212-11224, 10.1021/acs.est.2c00038, 2022a.





- Li, X., Qin, M., Li, L., Gong, K., Shen, H., Li, J., and Hu, J.: Examining the implications of photochemical indicators for O3-NOx-VOC sensitivity and control strategies: a case study in the
- 485 Yangtze River Delta (YRD), China, Atmos. Chem. Phys., 22, 14799-14811, 10.5194/acp-22-14799-2022, 2022b.
 - Liang, W. and Yang, X.: Indoor formaldehyde in real buildings: Emission source identification, overall emission rate estimation, concentration increase and decay patterns, BUILD ENVIRON., 69, 114-120, https://doi.org/10.1016/j.buildenv.2013.08.009, 2013.
- 490 Liu, Y., Zhou, M., Zhao, M., Jing, S., Wang, H., Lu, K., and Shen, H.: Determination of Urban Formaldehyde Emission Ratios in the Shanghai Megacity, Environ. Sci. Technol., 57, 16489-16499, 10.1021/acs.est.3c06428, 2023.
 - Liu, Y., Wang, H., Jing, S., Peng, Y., Gao, Y., Yan, R., Wang, Q., Lou, S., Cheng, T., and Huang, C.: Strong regional transport of volatile organic compounds (VOCs) during wintertime in Shanghai megacity
- of China, Atmos. Environ., 244, 117940, https://doi.org/10.1016/j.atmosenv.2020.117940, 2021.

 Liu, Y., Wang, H., Jing, S., Gao, Y., Peng, Y., Lou, S., Cheng, T., Tao, S., Li, L., Li, Y., Huang, D., Wang, Q., and An, J.: Characteristics and sources of volatile organic compounds (VOCs) in Shanghai during summer: Implications of regional transport, Atmos. Environ., 215, 116902,
- Luecken, D. J., Napelenok, S. L., Strum, M., Scheffe, R., and Phillips, S.: Sensitivity of Ambient Atmospheric Formaldehyde and Ozone to Precursor Species and Source Types Across the United States, Environ. Sci. Technol., 52, 4668-4675, 10.1021/acs.est.7b05509, 2018.

https://doi.org/10.1016/j.atmosenv.2019.116902, 2019.

- Lyu, X., Li, H., Lee, S.-C., Xiong, E., Guo, H., Wang, T., and de Gouw, J.: Significant Biogenic Source of Oxygenated Volatile Organic Compounds and the Impacts on Photochemistry at a Regional
- 505 Background Site in South China, Environ. Sci. Technol., 58, 20081-20090, 10.1021/acs.est.4c05656, 2024.
 - Ma, M., Gao, Y., Ding, A., Su, H., Liao, H., Wang, S., Wang, X., Zhao, B., Zhang, S., Fu, P., Guenther, A. B., Wang, M., Li, S., Chu, B., Yao, X., and Gao, H.: Development and Assessment of a High-Resolution Biogenic Emission Inventory from Urban Green Spaces in China, Environ. Sci. Technol., 56,
- 510 175-184, 10.1021/acs.est.1c06170, 2022.
 - Maison, A., Lugon, L., Park, S. J., Baudic, A., Cantrell, C., Couvidat, F., D'Anna, B., Di Biagio, C., Gratien, A., Gros, V., Kalalian, C., Kammer, J., Michoud, V., Petit, J. E., Shahin, M., Simon, L., Valari,





- M., Vigneron, J., Tuzet, A., and Sartelet, K.: Significant impact of urban tree biogenic emissions on air quality estimated by a bottom-up inventory and chemistry transport modeling, Atmos. Chem. Phys., 24,
- 515 6011-6046, 10.5194/acp-24-6011-2024, 2024.

6283-2015, 2015.

- Mao, J., Li, L., Li, J., Sulaymon, I. D., Xiong, K., Wang, K., Zhu, J., Chen, G., Ye, F., Zhang, N., Qin, Y., Qin, M., and Hu, J.: Evaluation of Long-Term Modeling Fine Particulate Matter and Ozone in China During 2013–2019, Front. Environ. Sci., 10 2022, 10.3389/fenvs.2022.872249, 2022.
- Marvin, M. R., Wolfe, G. M., Salawitch, R. J., Canty, T. P., Roberts, S. J., Travis, K. R., Aikin, K. C.,
- de Gouw, J. A., Graus, M., Hanisco, T. F., Holloway, J. S., Hübler, G., Kaiser, J., Keutsch, F. N., Peischl, J., Pollack, I. B., Roberts, J. M., Ryerson, T. B., Veres, P. R., and Warneke, C.: Impact of evolving isoprene mechanisms on simulated formaldehyde: An inter-comparison supported by in situ observations from SENEX, Atmos. Environ., 164, 325-336, https://doi.org/10.1016/j.atmosenv.2017.05.049, 2017.
 - McDonald, B. C., de Gouw, J. A., Gilman, J. B., Jathar, S. H., Akherati, A., Cappa, C. D., Jimenez, J. L.,
- Lee-Taylor, J., Hayes, P. L., McKeen, S. A., Cui, Y. Y., Kim, S.-W., Gentner, D. R., Isaacman-VanWertz, G., Goldstein, A. H., Harley, R. A., Frost, G. J., Roberts, J. M., Ryerson, T. B., and Trainer, M.: Volatile chemical products emerging as largest petrochemical source of urban organic emissions, Science, 359, 760-764, doi:10.1126/science.aaq0524, 2018.
- Millet, D. B., Baasandorj, M., Farmer, D. K., Thornton, J. A., Baumann, K., Brophy, P., Chaliyakunnel,
 S., de Gouw, J. A., Graus, M., Hu, L., Koss, A., Lee, B. H., Lopez-Hilfiker, F. D., Neuman, J. A., Paulot,
 F., Peischl, J., Pollack, I. B., Ryerson, T. B., Warneke, C., Williams, B. J., and Xu, J.: A large and ubiquitous source of atmospheric formic acid, Atmos. Chem. Phys., 15, 6283-6304, 10.5194/acp-15-
 - Mo, Z., Shao, M., and Lu, S.: Compilation of a source profile database for hydrocarbon and OVOC
- emissions in China, Atmos. Environ., 143, 209-217, https://doi.org/10.1016/j.atmosenv.2016.08.025, 2016.
 - Mo, Z., Cui, R., Yuan, B., Cai, H., McDonald, B. C., Li, M., Zheng, J., and Shao, M.: A mass-balance-based emission inventory of non-methane volatile organic compounds (NMVOCs) for solvent use in China, Atmos. Chem. Phys., 21, 13655-13666, 10.5194/acp-21-13655-2021, 2021.
- Niu, Z., Kong, S., Zheng, H., Hu, Y., Zheng, S., Cheng, Y., Yao, L., Liu, W., Ding, F., Liu, X., and Qi, S.: Differences in compositions and effects of VOCs from vehicle emission detected using various methods, Environ. Pollut., 333, 122077, https://doi.org/10.1016/j.envpol.2023.122077, 2023.





- Niu, Z., Kong, S., Zheng, H., Yan, Q., Liu, J., Feng, Y., Wu, J., Zheng, S., Zeng, X., Yao, L., Zhang, Y., Fan, Z., Cheng, Y., Liu, X., Wu, F., Qin, S., Yan, Y., Ding, F., Liu, W., Zhu, K., Liu, D., and Qi, S.:
- Temperature dependence of source profiles for volatile organic compounds from typical volatile emission sources, Sci. Total Environ., 751, 141741, https://doi.org/10.1016/j.scitotenv.2020.141741, 2021.
 - Ou, J., Zheng, J., Li, R., Huang, X., Zhong, Z., Zhong, L., and Lin, H.: Speciated OVOC and VOC emission inventories and their implications for reactivity-based ozone control strategy in the Pearl River
- 550 Delta region, China, Sci. Total Environ., 530-531, 393-402, https://doi.org/10.1016/j.scitotenv.2015.05.062, 2015.
 - Permar, W., Wielgasz, C., Jin, L., Chen, X., Coggon, M. M., Garofalo, L. A., Gkatzelis, G. I., Ketcherside, D., Millet, D. B., Palm, B. B., Peng, Q., Robinson, M. A., Thornton, J. A., Veres, P., Warneke, C., Yokelson, R. J., Fischer, E. V., and Hu, L.: Assessing formic and acetic acid emissions and chemistry in
- 555 western U.S. wildfire smoke: implications for atmospheric modeling, Environ. Sci.: Atmos., 3, 1620-1641, 10.1039/D3EA00098B, 2023.
 - Permar, W., Wang, Q., Selimovic, V., Wielgasz, C., Yokelson, R. J., Hornbrook, R. S., Hills, A. J., Apel, E. C., Ku, I.-T., Zhou, Y., Sive, B. C., Sullivan, A. P., Collett Jr, J. L., Campos, T. L., Palm, B. B., Peng, Q., Thornton, J. A., Garofalo, L. A., Farmer, D. K., Kreidenweis, S. M., Levin, E. J. T., DeMott, P. J.,
- Flocke, F., Fischer, E. V., and Hu, L.: Emissions of Trace Organic Gases From Western U.S. Wildfires Based on WE-CAN Aircraft Measurements, J. Geophys. Res. Atmos., 126, e2020JD033838, https://doi.org/10.1029/2020JD033838, 2021.
 - Pfannerstill, E. Y., Arata, C., Zhu, Q., Schulze, B. C., Woods, R., Harkins, C., Schwantes, R. H., McDonald, B. C., Seinfeld, J. H., Bucholtz, A., Cohen, R. C., and Goldstein, A. H.: Comparison between
- Spatially Resolved Airborne Flux Measurements and Emission Inventories of Volatile Organic Compounds in Los Angeles, Environ. Sci. Technol., 57, 15533-15545, 10.1021/acs.est.3c03162, 2023.

 Pusede, S. E., Gentner, D. R., Wooldridge, P. J., Browne, E. C., Rollins, A. W., Min, K. E., Russell, A.
 - R., Thomas, J., Zhang, L., Brune, W. H., Henry, S. B., DiGangi, J. P., Keutsch, F. N., Harrold, S. A.,
 - Thornton, J. A., Beaver, M. R., St. Clair, J. M., Wennberg, P. O., Sanders, J., Ren, X., VandenBoer, T.
- 570 C., Markovic, M. Z., Guha, A., Weber, R., Goldstein, A. H., and Cohen, R. C.: On the temperature dependence of organic reactivity, nitrogen oxides, ozone production, and the impact of emission controls





in San Joaquin Valley, California, Atmos. Chem. Phys., 14, 3373-3395, 10.5194/acp-14-3373-2014, 2014.

Qin, M. M., She, Y. L., Wang, M., Wang, H. L., Chang, Y. H., Tan, Z. F., An, J. Y., Huang, J., Yuan, Z.

- B., Lu, J., Wang, Q., Liu, C., Liu, Z. X., Xie, X. D., Li, J. Y., Liao, H., Pye, H. O. T., Huang, C., Guo, S., Hu, M., Zhang, Y. H., Jacob, D. J., and Hu, J. L.: Increased urban ozone in heatwaves due to temperature-induced emissions of anthropogenic volatile organic compounds, Nat. Geosci, 15, 10.1038/s41561-024-01608-w, 2025.
 - Qu, H., Wang, Y., Zhang, R., Liu, X., Huey, L. G., Sjostedt, S., Zeng, L., Lu, K., Wu, Y., Shao, M., Hu,
- M., Tan, Z., Fuchs, H., Broch, S., Wahner, A., Zhu, T., and Zhang, Y.: Chemical Production of Oxygenated Volatile Organic Compounds Strongly Enhances Boundary-Layer Oxidation Chemistry and Ozone Production, Environ. Sci. Technol., 55, 13718-13727, 10.1021/acs.est.1c04489, 2021.
 - Smith, S. J., McDuffie, E. E., and Charles, M.: Opinion: Coordinated development of emission inventories for climate forcers and air pollutants, Atmos. Chem. Phys., 22, 13201-13218, 10.5194/acp-
- 585 22-13201-2022, 2022.
 - Stockwell, C. E., Coggon, M. M., Gkatzelis, G. I., Ortega, J., McDonald, B. C., Peischl, J., Aikin, K., Gilman, J. B., Trainer, M., and Warneke, C.: Volatile organic compound emissions from solvent- and water-borne coatings compositional differences and tracer compound identifications, Atmos. Chem. Phys., 21, 6005-6022, 10.5194/acp-21-6005-2021, 2021.
- Tan, Z., Lu, K., Hofzumahaus, A., Fuchs, H., Bohn, B., Holland, F., Liu, Y., Rohrer, F., Shao, M., Sun, K., Wu, Y., Zeng, L., Zhang, Y., Zou, Q., Kiendler-Scharr, A., Wahner, A., and Zhang, Y.: Experimental budgets of OH, HO2, and RO2 radicals and implications for ozone formation in the Pearl River Delta in China 2014, Atmos. Chem. Phys., 19, 7129-7150, 10.5194/acp-19-7129-2019, 2019a.
 - Tan, Z. F., Lu, K. D., Jiang, M. Q., Su, R., Wang, H. L., Lou, S. R., Fu, Q. Y., Zhai, C. Z., Tan, Q. W.,
- Yue, D. L., Chen, D. H., Wang, Z. S., Xie, S. D., Zeng, L. M., and Zhang, Y. H.: Daytime atmospheric oxidation capacity in four Chinese megacities during the photochemically polluted season: a case study based on box model simulation, Atmos. Chem. Phys., 19, 3493-3513, 10.5194/acp-19-3493-2019, 2019b. Wang, H., He, Q., Kong, H., Qin, K., Zheng, B., Lin, J., and Zhao, Y.: Declining short-term emission control opportunity for major events in Chinese cities, Nat. Cities, 2, 434-446, 10.1038/s44284-025-
- 600 00233-x, 2025.





- Wang, J., Zhang, Y., Zhao, W., Wu, Z., Luo, S., Zhang, H., Zhou, H., Song, W., Zhang, W., and Wang, X.: Observationally Constrained Modeling of Peroxy Radical During an Ozone Episode in the Pearl River Delta Region, China, J. Geophys. Res. Atmos., 128, e2022JD038279, https://doi.org/10.1029/2022JD038279, 2023.
- Wang, S., Yuan, B., He, X., Cui, R., Song, X., Chen, Y., Wu, C., Wang, C., Huangfu, Y., Li, X. B., Wang, B., and Shao, M.: Emission characteristics of reactive organic gases (ROGs) from industrial volatile chemical products (VCPs) in the Pearl River Delta (PRD), China, Atmos. Chem. Phys., 24, 7101-7121, 10.5194/acp-24-7101-2024, 2024a.
 - Wang, S., Yuan, B., Wu, C., Wang, C., Li, T., He, X., Huangfu, Y., Qi, J., Li, X. B., Sha, Q., Zhu, M.,
- 610 Lou, S., Wang, H., Karl, T., Graus, M., Yuan, Z., and Shao, M.: Oxygenated volatile organic compounds (VOCs) as significant but varied contributors to VOC emissions from vehicles, Atmos. Chem. Phys., 22, 9703-9720, 10.5194/acp-22-9703-2022, 2022a.
 - Wang, W., Yuan, B., Peng, Y., Su, H., Cheng, Y., Yang, S., Wu, C., Qi, J., Bao, F., Huangfu, Y., Wang, C., Ye, C., Wang, Z., Wang, B., Wang, X., Song, W., Hu, W., Cheng, P., Zhu, M., Zheng, J., and Shao,
- M.: Direct observations indicate photodegradable oxygenated volatile organic compounds (OVOCs) as larger contributors to radicals and ozone production in the atmosphere, Atmos. Chem. Phys., 22, 4117-4128, 10.5194/acp-22-4117-2022, 2022b.
 - Wang, Y., Huang, J., Zhao, B., Du, Y., Huang, L., Lai, D., Su, Q., Manomaiphiboon, K., and Li, L.: Full-Volatility Reactive Organic Carbon Emissions from Volatile Chemical Products in Mainland China, ACS
- Wiedinmyer, C., Kimura, Y., McDonald-Buller, E. C., Emmons, L. K., Buchholz, R. R., Tang, W., Seto, K., Joseph, M. B., Barsanti, K. C., Carlton, A. G., and Yokelson, R.: The Fire Inventory from NCAR version 2.5: an updated global fire emissions model for climate and chemistry applications, Geosci.
 - Model Dev., 16, 3873-3891, 10.5194/gmd-16-3873-2023, 2023.

ES&T Air, 1, 1541-1553, 10.1021/acsestair.4c00116, 2024b.

Wu, C., Wang, C., Wang, S., Wang, W., Yuan, B., Qi, J., Wang, B., Wang, H., Wang, C., Song, W., Wang, X., Hu, W., Lou, S., Ye, C., Peng, Y., Wang, Z., Huangfu, Y., Xie, Y., Zhu, M., Zheng, J., Wang, X., Jiang, B., Zhang, Z., and Shao, M.: Measurement report: Important contributions of oxygenated compounds to emissions and chemistry of volatile organic compounds in urban air, Atmos. Chem. Phys., 20, 14769-14785, 10.5194/acp-20-14769-2020, 2020.





- Xing, C., Liu, C., Lin, J., Tan, W., and Liu, T.: VOCs hyperspectral imaging: A new insight into evaluate emissions and the corresponding health risk from industries, J. Hazard. Mater., 461, 132573, https://doi.org/10.1016/j.jhazmat.2023.132573, 2024.
 - Xue, L., Gu, R., Wang, T., Wang, X., Saunders, S., Blake, D., Louie, P. K. K., Luk, C. W. Y., Simpson, I., Xu, Z., Wang, Z., Gao, Y., Lee, S., Mellouki, A., and Wang, W.: Oxidative capacity and radical
- chemistry in the polluted atmosphere of Hong Kong and Pearl River Delta region: analysis of a severe photochemical smog episode, Atmos. Chem. Phys., 16, 9891-9903, 10.5194/acp-16-9891-2016, 2016. Yang, X., Zhang, G., Pan, G., Fan, G. L., Zhang, H. Y., Ge, X., and Du, M. Y.: Significant contribution of carbonyls to atmospheric oxidation capacity (AOC) during the winter haze pollution over North China Plain, J. Environ. Sci., 139, 377-388, 10.1016/j.jes.2023.06.004, 2024.
- Yang, X., Xue, L., Wang, T., Wang, X., Gao, J., Lee, S., Blake, D. R., Chai, F., and Wang, W.: Observations and Explicit Modeling of Summertime Carbonyl Formation in Beijing: Identification of Key Precursor Species and Their Impact on Atmospheric Oxidation Chemistry, J. Geophys. Res. Atmos., 123, 1426-1440, 10.1002/2017jd027403, 2018.
 - Yang, X., Lu, K., Ma, X., Gao, Y., Tan, Z., Wang, H., Chen, X., Li, X., Huang, X., He, L., Tang, M.,
- Zhu, B., Chen, S., Dong, H., Zeng, L., and Zhang, Y.: Radical chemistry in the Pearl River Delta: observations and modeling of OH and HO2 radicals in Shenzhen in 2018, Atmos. Chem. Phys., 22, 12525-12542, 10.5194/acp-22-12525-2022, 2022.
 - Yuan, B., Veres, P. R., Warneke, C., Roberts, J. M., Gilman, J. B., Koss, A., Edwards, P. M., Graus, M., Kuster, W. C., Li, S. M., Wild, R. J., Brown, S. S., Dubé, W. P., Lerner, B. M., Williams, E. J., Johnson,
- J. E., Quinn, P. K., Bates, T. S., Lefer, B., Hayes, P. L., Jimenez, J. L., Weber, R. J., Zamora, R., Ervens, B., Millet, D. B., Rappenglück, B., and de Gouw, J. A.: Investigation of secondary formation of formic acid: urban environment vs. oil and gas producing region, Atmos. Chem. Phys., 15, 1975-1993, 10.5194/acp-15-1975-2015, 2015.
- Zhu, J., Wang, S., Gu, C., Jiang, Z., Zhang, S., Xue, R., Yan, Y., and Zhou, B.: Why did ozone concentrations remain high during Shanghai's static management? A statistical and radical-chemistry perspective, Atmos. Chem. Phys., 24, 8383-8395, 10.5194/acp-24-8383-2024, 2024.